Paper:
Pan-Castillo, B., Gazze, S., Thomas, S., Lucas, C., Margarit, L., Gonzalez, D., Francis, L. & Conlan, R. (2018). Morphophysical dynamics of human endometrial cells during decidualization. *Nanomedicine: Nanotechnology, Biology and Medicine, 14*(7), 2235-2245.
http://dx.doi.org/10.1016/J.NANO.2018.07.004

Open Access funded by Natural Environment Research Council Under a Creative Commons license.

Nanomedicine: Nanotechnology, Biology, and Medicine
14 (2018) 2235–2245

nanomedicine
Nanotechnology, Biology, and Medicine

nanomedjournal.com

Morphophysical dynamics of human endometrial cells during decidualization

Belen Pan-Castillo, PhD[a,1], Salvatore A. Gazze, PhD[a,1], Samantha Thomas, BSc[a], Christopher Lucas, PhD[a], Lavinia Margarit, PhD[a,b], Deyarina Gonzalez, PhD[a], Lewis W. Francis, PhD[a], Robert Steven Conlan, PhD[a,*]

[a]*Swansea University Medical School, Singleton Park, Swansea, UK*
[b]*Princess of Wales Hospital, Bridgend, UK*

Received 5 May 2018; accepted 2 July 2018

Abstract

During decidualization, human mesenchymal-like endometrial stromal cells undergo well characterized cellular and molecular transformations in preparation for accepting a developing embryo. Modulation of cellular biophysical properties during decidualization is likely to be important in receptivity and support of the embryo in the uterus. Here we assess the biophysical properties of human endometrial stromal cells including topography, roughness, adhesiveness and stiffness in cells undergoing *in vitro* decidualization. A significant reduction in cell stiffness and surface roughness was observed following decidualization. These morphodynamical changes have been shown to be associated with alterations in cellular behavior and homeostasis, suggesting that localized endometrial cell biophysical properties play a role in embryo implantation and pregnancy. This cell–cell communication process is thought to restrict trophoblast invasion beyond the endometrial stroma, be essential in the establishment of pregnancy, and demonstrate the altered endometrial dynamics affecting cell–cell contact and migration regimes at this crucial interface in human reproduction.

Key words: Decidualization; Atomic force microscopy; Nanomechanics

Decidualization is a biological transformation process that closely resembles a mesenchymal–epithelial transition (MET), occurring independently of the presence of an implanting blastocyst. Decidualizing cells differentiate from elongated fibroblast-like endometrial stromal cells (ESCs) into a more rounded and highly specialized secretory epithelioid cell type, termed decidual cells.[1] Decidualizing ESCs undergo further morphological and biochemical alterations, including an expansion of the rough endoplasmic reticulum and Golgi complex, accumulation of glycogen and lipid droplets in the cytoplasm, enhanced expression of certain extracellular matrix proteins (laminin, type IV collagen, fibronectin, heparin sulfate), and an increase in the production of secretory proteins including prolactin (PRL) and insulin-like growth factor binding protein-1 (IGFBP-1), two established markers of decidualization.[2,3] Decidualization is also characterized by the growth of uterine spiral arteries and stromal infiltration by macrophages, large granular lymphocytes and uterine natural killer cells; regulating endovascular trophoblast invasion and the formation of a functional feto-maternal interface receptive to the semiallogeneic embryo.[4,5]

Decidualization occurs during the late secretory phase (day 23–28) of the menstrual cycle, when the uterus is primed for embryo attachment, and is a prerequisite for successful blastocyst implantation.[6] It is during this process that ESCs

This work was supported by the Natural and Environmental Research Council, UK [grant number NE/K004212/1]; and the Ser Cymru Life Science National Research Network, Wales, UK.

*Corresponding author.
E-mail address: r.s.conlan@swansea.ac.uk (R.S. Conlan).

[1] These authors equally contributed to the manuscript.

https://doi.org/10.1016/j.nano.2018.07.004

acquire specific functions related to recognition, selection, and acceptance of the allogeneic embryo, as well as the development of maternal immune tolerance. Any disturbance in the decidualization process could cause pregnancy complications such as implantation failure and pregnancy loss, infertility, aberrant endometrial receptivity, recurrent miscarriages, placental abruption and intrauterine fetal growth restriction.[7,8]

The molecular mechanisms governing decidualization are driven by increased levels of progesterone. Elevated progesterone stimulates an increase in the intracellular secondary messenger, cyclic adenosine monophosphate (cAMP), which sensitizes stromal cells to progesterone through activation of the protein kinase A (PKA) pathway, and subsequent activation of progesterone receptor targets involved in the decidualization process.[8–10] During this MET, mesenchymal cells are transformed, losing their front–rear polarity and acquiring epithelial apical–basal polarity characteristics. N-cadherin expression is replaced by E-cadherin, vimentin levels decrease and Snail expression is increased.[11,12]

Despite its importance, our understanding of the decidualization process remains limited. In particular, any consideration of how the physical characteristics of decidual ESCs could influence their function remains to be determined. Physical properties of cells are known to play important roles in motility, migration, proliferation and cell–cell contact, where they influence cellular behavior, embryonic development, homeostasis and disease progression.[13] Here we have characterized dynamic changes in the morphophysical traits of human ESCs that occur during the decidualization process. Primary stromal cells were isolated from the endometrium of fertile patients and treated *in vitro* with cAMP and progesterone to trigger decidualization, a process monitored by changes in cell shape and expression levels of PRL and IGFBP1, as well as EGFR which is known to associate in adhesion clusters. A number of physical measurements were made on live cells in close-to-physiological conditions using Atomic Force Microscopy (AFM), namely cell topography and roughness, cell adhesiveness and stiffness. A significant decrease in cell stiffness was observed, concomitant with decreased membrane roughness in cells that had undergone successful decidualization. These morphodynamical changes suggest that localized biomechanical markers confer decidual plasticity to endometrial cells, supporting embryo implantation and the maintenance of pregnancy.

Methods

Patients

Endometrial biopsies were obtained from women with proven fertility and regular menstrual cycles (patients having surgery for conditions other than infertility). The phase of the natural menstrual cycle was confirmed by ultrasound and histological criteria.[14] The inclusion criteria for this study were women of age 18–40 years, non-smokers, BMI < 30 and regular spontaneous ovulatory cycles which were confirmed with luteal phase serum progesterone levels (>30 nmol/L measured at the time of endometrial sampling). Luteinizing hormone (LH) urinary surge was also documented to direct the timing of Pipelle® endometrial biopsy collection (at LH + 7). Only those samples agreed to be in-date (with a maturation delay of <2 days) were included in the study. All patients had not received exogenous hormonal therapy for at least 2 months prior to the procedure. Women with systemic diseases or sexually transmitted infections were excluded from the study. Samples with evidence of endometritis, endometrial hyperplasia and endometrial polyps were also excluded from the study. Ethical approval was obtained from the South West Wales Research Ethics Committee at Abertawe Bro Morgannwg University Trust Health Board (ABMUHB) (LREC 05/WMW02/103); written consent was obtained from all patients at the time of recruitment.

Cell culture

Isolation of stromal cells from endometrial biopsies was performed as described.[15] ESCs were plated into a 35 mm FluoroDish cell culture dish (FluoroDish, World Precision Instruments, Sarasota, FL, USA) at a density of 3×10^5cells/dish, and maintained in DMEM/F12 with 10% FBS, 1% penicillin/streptomycin, 1 mM sodium pyruvate and 1 mM sodium bicarbonate at 37 °C under 5% CO_2 in humidified air.

Decidualization of human endometrial stromal cells

Confluent cells were washed twice in PBS and maintained in DMEM/F12 medium supplemented with 10% charcoal stripped media for 24 h prior to the start of the experiment. To induce decidualization, cells cultured in charcoal stripped media were treated with medroxyprogesterone acetate (MPA) (1 μM) and cAMP (0.5 mM) for 96 h and maintained as detailed previously. Decidualization was evaluated by analyzing changes in cell morphology, and by measuring the secreted levels of IGFBP-1 and decidual PRL (dPRL) in the cell culture media.

Morphological analysis of decidualized ESCs using shape descriptors

Morphological changes of ESCs after successful induction of decidualization were analyzed using ImageJ software[16] using images taken at various time points of the cell monolayers. Changes in shape descriptors corresponding to area, circularity and roundness were selected as positive indicators of decidualization. 'Area' represents the total pixel area measured and converted to μm for the analysis. Shape index was calculated using two descriptors, circularity and roundness, where a shape index of 1.0 corresponds to a perfect round circle, and a value approaching 0.0 indicates an increasingly elongated shape.

Circularity was calculated using the following equation:

$$Circularity = 4\pi \frac{[Area]}{[Perimeter]^2}$$

Whereas roundness was calculated using the following equation:

$$Roundness = 4\ x\ \frac{[Area]}{\pi\ x\ [Major\ axis]^2}$$

Cellular shape indexes were calculated using twenty cells per treatment group, and from two independent experiments.

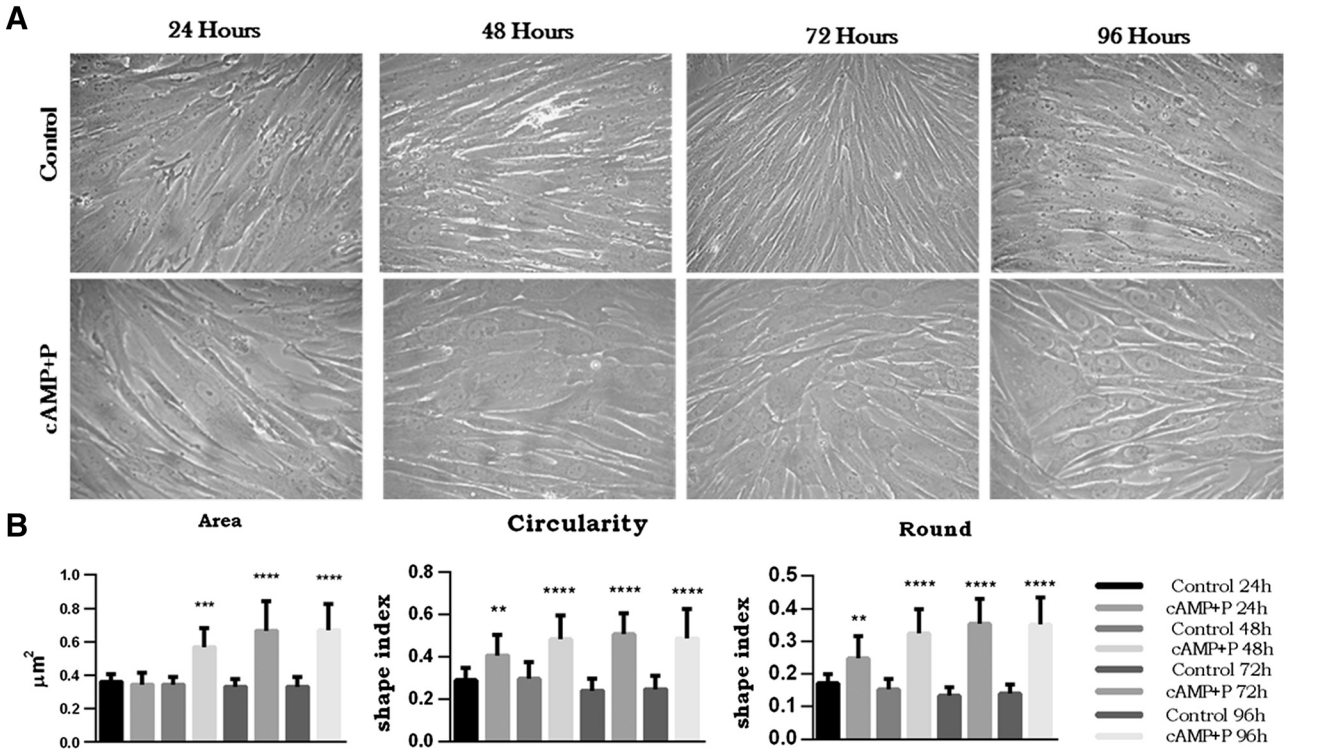

Figure 1. Morphological changes induced by decidualization in endometrial stromal cells. **(A)** Images from ESCs in which decidualization was induced by combined treatment of cAMP and progesterone (MPA) and compared with untreated control cells at time points indicated. **(B)** Area of decidualized ESCs and untreated cells shows that after 24 h of treatment decidualized ESCs were significantly larger than control cells ($P < 0.001$). Round and circularity shape indices in treated and untreated ESCs indicate that after 24 h, successful decidualization of ESCs is already taking place ($P < 0.01$) and this effect is more pronounced at 72 h ($P < 0.001$).

Measurement of secreted IGFBP-1 and PRL in culture media by ELISA

Concentrations of secreted IGFBP-1 and dPRL in cell culture media were measured using commercial ELISA kits according to the manufacturer's instructions (DY871, DY682; R&D systems). Measurements were performed in triplicate and at various time points.

Protein blotting

Total cellular protein was extracted using TRIzol™ reagent (Invitrogen Ltd., UK) and quantified using the *DC*™ Protein Assay (BioRad, UK). Protein from each sample was mixed with Laemmli sample buffer containing β-mercaptoethanol (5%) and boiled at 95 °C for 5 min. Equal amounts of protein were separated by SDS-PAGE (10% gels) and subsequently transferred onto a PVDF membrane (Amersham Pharmacia Biotech., UK). The membranes were blocked overnight in 5% non-fat milk prepared in 0.1% TBS-Tween20® (TBS-T). Blots were then incubated with the corresponding primary antibody (E-cadherin: rabbit polyclonal, Vimentin: mouse polyclonal, Pan Cytokeratin: mouse monoclonal or GAPDH: rabbit polyclonal) at a concentration of 200 μg/ml for 1 h and subsequently for 45 min with the appropriate secondary antibody (Goat anti-mouse or Goat anti-rabbit HRP-secondary) at a concentration of 400 μg/ml. For signal detection, membranes were processed using the Clarity™ Western ECL Substrate kit according to the manufacturer's recommendations and visualized using a ChemiDoc XRS system (BioRad, UK).

Quantitative real-time PCR

Following RNA extraction and quantification, qPCR was carried out in accordance to the manufacturers' recommendations using the RETROscript® (Invitrogen Ltd., UK) two-step method. Each sample was then analyzed by qPCR in triplicate using iQ SYBR Green supermix (BioRad, UK) and gene specific primers to evaluate EGFR expression (**EGFR F**: TGAACTGACTTCCGCAAG**, EGFR R:** GTGAACCCTCAGCCAATC**)** and GAPDH (**GAPDH F**: GTCCACTGGCGTCTTCAC**, GAPDH R**: CTTGAGGCTGTTGTCATACTTC). Serial dilutions of cDNA were used to plot a calibration curve, and gene expression was quantified by plotting threshold cycle values. Expression levels were normalized to values obtained for the reference gene. Relative expression was expressed as the mean fold induction ± standard deviation. Statistical differences between the treatment groups and the control were determined by analysis of variance (ANOVA) (where $P < 0.05$ was considered significant).

Confocal microscopy

ESCs were grown to 80% confluence on chamber slides (Thermo Scientific Ltd., UK) in 100 mm plates. At 96 h post induction of decidualization, cells were fixed with 4% paraformaldehyde and permeabilized with 0.01% Triton X-100 (Sigma, UK), both dissolved in PBS, and consequently blocked in 5% donkey serum (Invitrogen Ltd., UK) and 1% BSA for 1 h. Primary antibody (E-cadherin: rabbit polyclonal, Vimentin:

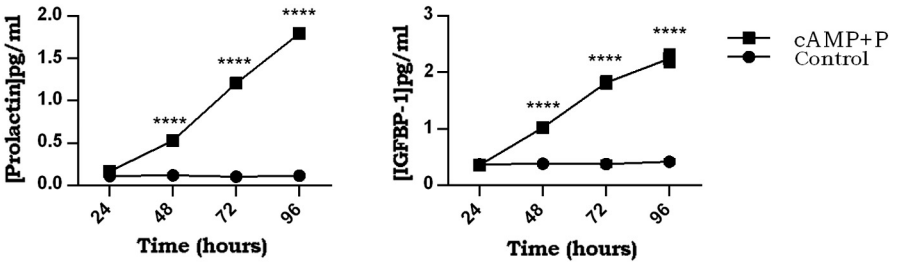

Figure 2. Prolactin and IGFBP-1 secretion by decidualized endometrial stromal cells. Endometrial stromal cells were co-treated with MPA and cAMP for 96 h. The secretion levels of PRL and IGFBP-1 were determined by ELISA at 24 h time points. **(Left)** After 24 h, secretion of prolactin was significantly increased compared to the control ($P < 0.001$). **(Right)** Secreted IGFBP-1 levels were significantly increased at each time point compared with untreated cells ($P < 0.001$).

mouse polyclonal and Pan Cytokeratin: mouse monoclonal) was added at a concentration of 200 μg/ml and incubated overnight, removed by washing in PBS and secondary antibody was then added. Following staining with DAPI (Vectashield, UK) cells were imaged using a LSM710 confocal fluorescence microscope system (Zeiss, UK).

Atomic force microscopy (AFM)

Cells were analyzed using a BioScope Catalyst (Bruker Instruments, USA) mounted a Nikon Eclipse Ti-S inverted optical microscope (Nikon Instruments, Netherlands). During AFM, cells were kept alive in buffer at 37 °C in a petri dish using a heater stage connected to Bruker/LakeShore 331S Temperature Controller and analyzed for a maximum of 3 h. The inverted optical microscope was used to carefully position the tip on the desired cell and to visually evaluate the decidualized state before AFM analysis (Supplementary Figure 1). Topography data were obtained in Peak Force Tapping mode using MLCT silicon nitride cantilevers (Bruker nano, Coventry, UK). The roughness was measured on 70 areas of 25 μm^2 each on five cells for both control and decidualized cells. The roughness subroutine in the Nanoscope Analysis software v1.50 was adopted, which calculates roughness using Eq. (1):

$$R_{RMS} = \sqrt{\frac{\sum Z_i^2}{N}} \tag{1}$$

In Eq. (1), N is the number of height points in the analyzed area and Z_i is the vertical distance of data point i from the mean image data plane.

Nanomechanics measurements were conducted using both sharp and colloidal probes: Bruker MLCT-D silicon nitride cantilevers were used for sharp probes, with a nominal tip radius of 20 nm and a nominal spring constant of 0.03 N/m; for colloidal probes Novascan cantilevers were used, with a nominal spring constant of 0.35 N/m and a borosilicate spheric probe with a radius of 2.5 μm. Prior to measurements, deflection sensitivity and spring constant were experimentally determined, the latter using the thermal tune subroutine of the Nanoscope software. Force curves were taken on 10-15 cells for both control and decidualized cells: on each cell, 25 force curves equally spaced were acquired on an area of 100 μm^2 away from the cell boundary edges and the nucleus region. Force curves were acquired with a ramp rate of 1 Hz and a ramp size of 1 μm and 1.5 μm for sharp and colloidal probes, respectively. The approach curve in the contact regime of each force curve was fitted using two distinct models: for sharp probes, a conical model (Sneddon model, Eq. (2a)) was adopted since the indentation depth exceeded the probe radius (20 nm), while for colloidal probes the classical Hertz model was used, Eq. (2b). In both cases, the fitting module in the Nanoscope Analysis software v1.50 was used and only curves with a goodness of fit between 0.85 and 1 were considered for statistical analysis.

$$F = \frac{2\ E\ \tan(\alpha)\delta^2\sqrt{R}}{\pi\ (1-\upsilon^2)} \tag{2a}$$

$$F = \frac{4E\sqrt{R}\,\delta^{3/2}}{3\ (1-\upsilon^2)} \tag{2b}$$

In Eqs. (2a) and (2b), F is the force applied by the cantilever tip to the cell, E is the Young's modulus (fit parameter), υ is the Poissons ratio (0.5), R the radius of the indenter, δ is the indentation depth and α is the half-angle of the indenter (18° for the used sharp probes). For both probes types, a force of 200 pN has been used. For adhesion measurements, the "snap-off" force for each retraction curve was considered.

Statistical analysis

Normality of the data was analyzed using the Kolmogorov Smirnov test. Normally distributed data were analyzed with the one-way and two-way analysis of variance (ANOVA) and the Mann–Whitney test for non-parametric data. In all cases in which ANOVA was significant, multiple comparison methods were used. Differences were considered significant for $P \leq 0.05$ ($*P \leq 0.05$, $**P \leq 0.01$, $***P \leq 0.001$, $****P \leq 0.0001$). All data were analyzed using GraphPad Prism 6, MiniTab 14 and Mathematica 10.

Results

Decidualization induces morphological changes in human endometrial stromal cells

A defining feature of decidualization is the morphological change induced in ESCs, which includes the acquisition of a

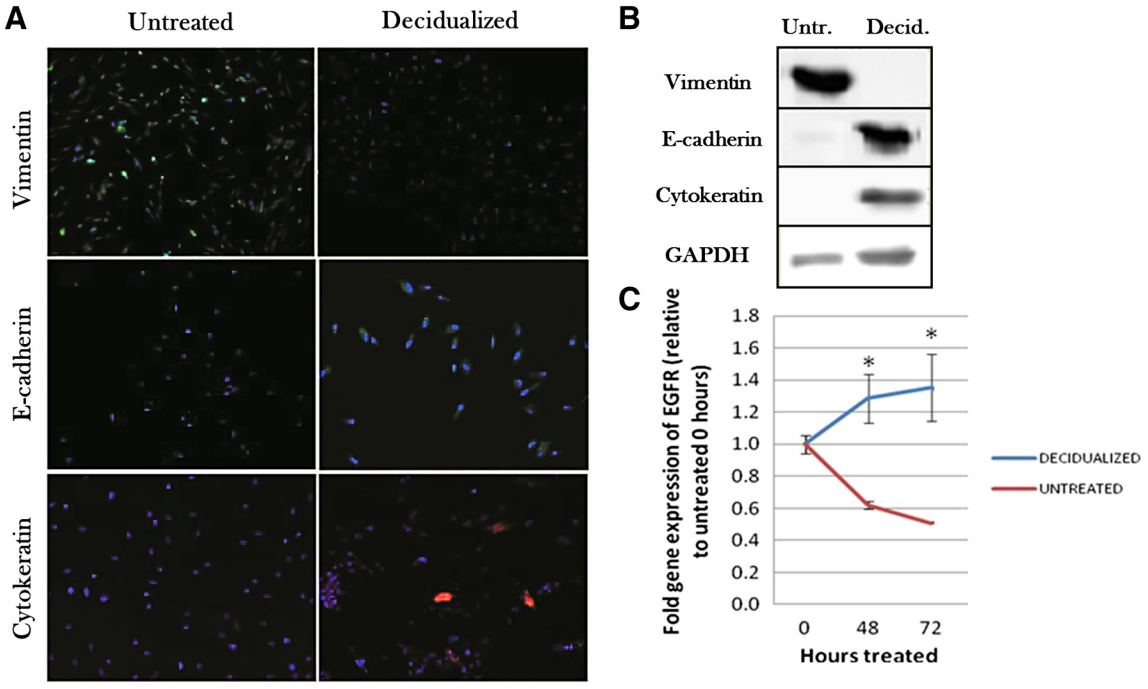

Figure 3. Alterations in vimentin, E-cadherin, cytokeratin and EGFR expression at both the protein and RNA level demonstrate Mesenchymal to Epithelial transition (MET) in ESCs. **(A)** Protein expression of vimentin (green), E-cadherin (green) and cytokeratin (red) were detected by confocal microscopy in untreated and decidualized ESCs at 96 h. **(B)** Protein extracts from untreated and decidualized ESCs at 96 h were analyzed by western blot to measure the expression of vimentin, E-cadherin, cytokeratin and GAPDH. **(C)** Gene expression of EGFR was measured by qPCR and revealed an increase in expression in decidualized cells compared with the untreated control.

rounded shape, cobblestone morphology with concomitant increase in cell area. Cell circularity, roundness and area were used to quantify changes in cell morphology upon successful decidualization (Figure 1, *A*). In decidualized ESCs, a statistically significant increase in the shape indices of circularity and roundness was observed at all considered time points compared to controls, while a significant increase in total cell area was detected only after 48 h ($P < 0.001$) (Figure 1, *B*, $P < 0.0001$). A stabilization of all three indices, which mark the decidualization progression, was obtained approximately after 72 h. dPRL and IGFBP-1, which are known markers of decidualization, increase in expression in the epithelial and stromal cell region of the endometrium, starting in the secretory phase of the menstrual cycle, and usually increase in the first trimester of pregnancy. dPRL and IGFBP-1 secretion levels were measured throughout the experiment, and were increased significantly after 24 h of exposure to the *in vitro* decidualization stimulus compared to untreated controls (Figure 2, $P < 0.0001$), therefore confirming a decidual response.

Mesenchymal to epithelial transition of ESCs during in vitro decidualization

Decidualization was induced in ESCs and expression of various mesenchymal to epithelial transition-markers (cytokeratin, vinculin, and E-cadherin) was determined in order to evaluate whether the process was truly representative of MET. In control ESCs, vimentin expression levels were high, while it was undetectable in decidualized cells (Figure 3, $P < 0.001$). Expression of both E-cadherin and cytokeratin was very low in untreated control ESCs whereas both were increased significantly following treatment to induce *in vitro* decidualization ($P < 0.001$), demonstrating the MET nature of decidual transformation. In addition, an increase in the levels of EGFR, a key regulator of decidual signaling events, was observed, further confirming decidualization.

Decidualized cells exhibit altered morphology and topography

Using AFM we conducted multi-parameter analysis of ESCs during the decidualization process, to determine morphodynamic cellular alterations that could influence cellular behavior. Analysis of ESC topography confirmed the population level circularity data, demonstrating an induction of a distinct transformation in cell morphology after treatment for 48 h with cells showing a more rounded and epithelial-like outline (Figure 4, *C*). High resolution imaging provided further insights into how individual decidualized cells interact with neighboring cells, as well as with the underlying glass substrate. In Figure 4, *C*, for example, the lower half of the cell interacts with nearby cells through relatively flat cell surface extensions, which are seemingly stabilized by fibrillary cytoskeleton structures. The upper part of the cell appears to utilize a more localized cell membrane extrusion to firmly adhere to the substrate, a phenomenon observed consistently throughout the cultures at high resolution.

Peak Force Error image data resolved differential cytoskeletal organization underlying the cell membrane: large stress fibers were observed in the control cells (Figure 4, *B*), while more

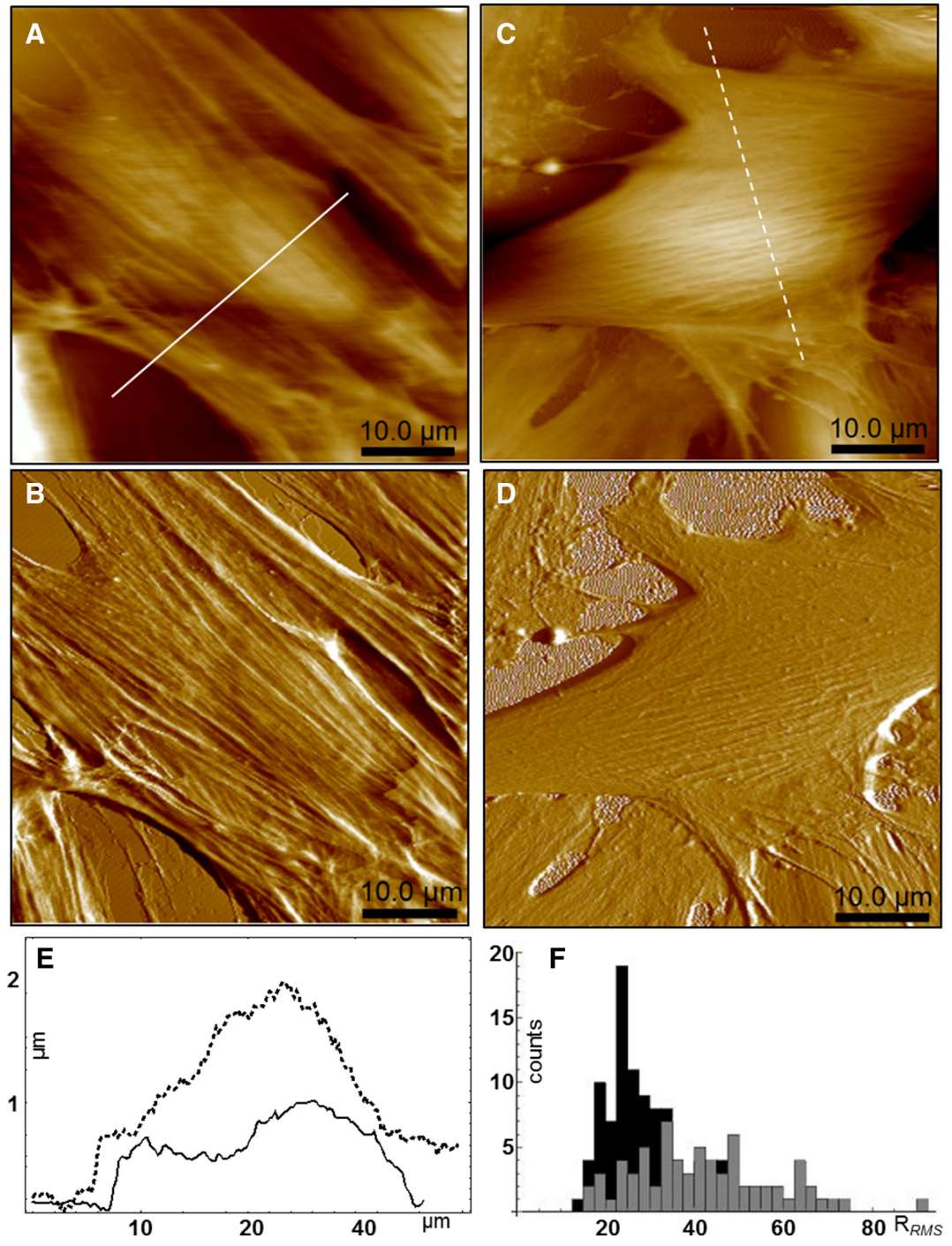

Figure 4. Decidualized cell morphology and topography. High resolution, live cell QNM imaging was performed using AFM and subsequent image analysis revealed morphological and topographical cell changes during decidualization after 48 h incubation with the *in vitro* decidualization stimuli. Control **(A** and **B)** and decidualized **(C** and **D)** ESCs are shown with height and Peak Force error signals respectively. The underlying cytoskeleton is visualized more prominently in the control cells. Height line profiles across the cell surface **(E)** are shown for both control (dark, continuous line) and decidualized cells (dotted line), indicating greater cell height in the treated cells. **(F)** Cell surface roughness was calculated on seventy 25 μm^2 areas in both study groups. Control cell surface roughness (R_{RMS} (gray) = 41.3 ± 1.9 nm) was significantly higher than that observed in decidualized cells (R_{RMS} (black) = 27.2 ± 1.1 nm) ($P < 0.0001$).

densely packed, thinner fibers were clear in the decidualized cells (Figure 4, *D*). The height of decidualized cells was at least double that of untreated cells (Figure 4, *E*), and resulted in a significant lower height to width with respect to untreated cells, 19.0 ± 0.7 and 30.3 ± 3.4, respectively ($P \leq 0.05$). A change of surface roughness was also observed. A component of surface texture, surface roughness (R_{RMS}) is quantified by the deviations in image height profile in a given geometric area.

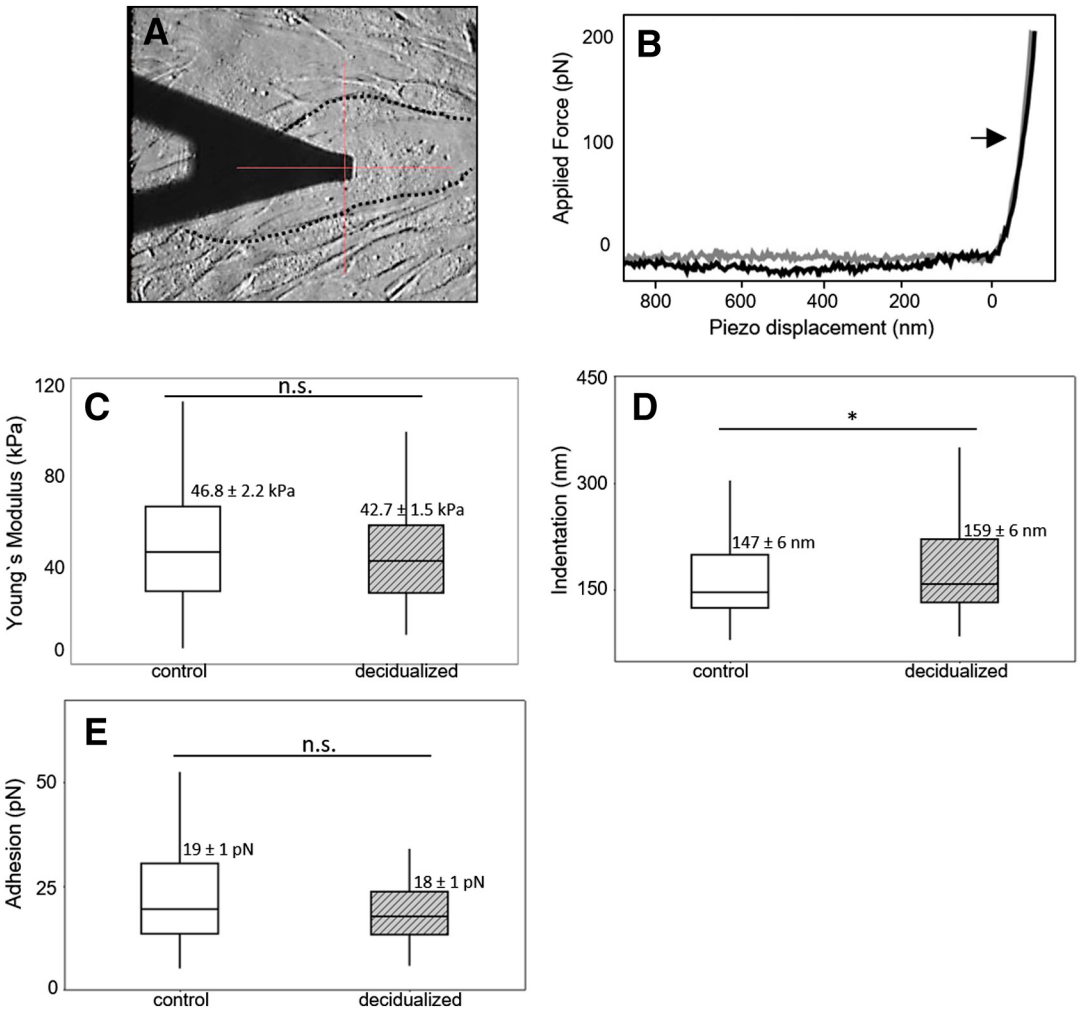

Figure 5. Decidualization with sharp tips and 200 pN applied force. An AFM probe with a sharp tip, carefully positioned away from the cell boundary edges and the nucleus region **(A)**, was used as a nanoindentor to monitor changes in cell elasticity following decidualization. Using standard hertzian mechanics, elasticity was calculated from the observed changes in the contact regime of the force curve (arrow in panel **B**), where two example approach curves are depicted here, on a control ESC (gray) and on a successfully decidualized cell (black). The 0 point in the x-axis indicates when the cantilever tip makes contact with the cell surface **(B)**. Total cell elasticity values are depicted in boxplots for control and decidualized cells at 72 h. **(C)** No significant alteration in median value ($P > 0.05$) was detected between control (46.8 ± 2.2 kPa) and decidualized cells (42.7 ± 1.5 kPa). Indentation data are reported in **D**, where applying the same force results in decidualized cells deforming more than control cells (159 ± 6 nm and 147 ± 6 nm respectively) ($P < 0.05$). **(E)** Cantilever pull-off adhesion force, where both groups display non-specific stickiness properties ($P > 0.05$). Statistical significance was determined using the Mann–Whitney test, with the following used symbols: ns = $P > 0.05$ (threshold P value = 0.05); * = $P \leq 0.05$; ** = $P \leq 0.01$; *** = $P \leq 0.001$; **** = $P \leq 0.0001$.

Decidualization resulted in significantly decreased $R_{RMS,}$ with values of 27.2 ± 1.1 nm in decidualized cells compared to 41.3 ± 1.9 nm in the untreated cells ($P < 0.0001$), Figure 4, *F*.

Decidualized cells exhibit an altered physical and mechanical phenotype

AFM imaging indicated that decidual induction resulted in coalescence and re-polarization of ESCs, and the establishment of an epithelial phenotype following a MET process. Alongside the specific changes in cell shape and morphology, distinct morphophysical and mechanical changes associated with cytoskeletal filament re-organization were observed. Using the AFM probe as a force nanoindentor, AFM force curves were acquired in cellular regions away from the nuclear area and the cell boundaries for both control and decidualized cells after 72 h treatment with MPA and cAMP. This time point was chosen as it is when most of the morphological changes stabilized (Figure 1) and hence were likely accompanied with significant changes in biophysical traits. Using sharp tips and applying a force of 200 pN (Figure 5, *C*), no significant alteration in cellular elastic moduli was observed ($P > 0.05$). Indentation data, however, showed a significant increase in surface deformation of decidualized (159 ± 6 nm) compared to control cells (147 ± 6 nm; $P < 0.05$), Figure 5, *D*, indicating a softening of the cell associated with the decidualization process. No significant alterations in cellular adhesion were detected during decidualization (Figure 5, *E*).

Decidualized cells probed with a colloidal indentor (2.5 μm radius) and using the same applied force (200 pN) exhibited

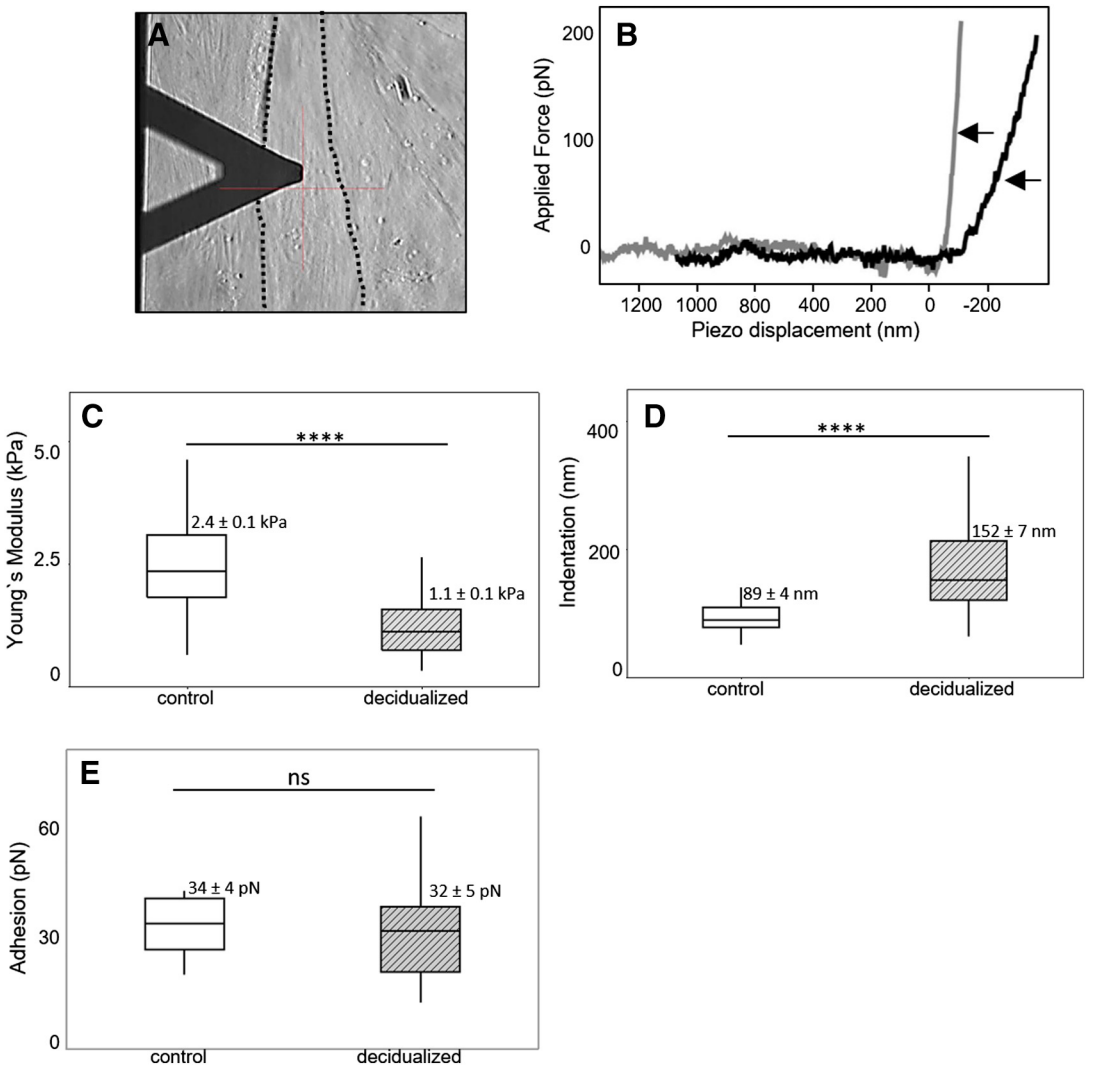

Figure 6. Decidualization with colloidal probes and 200 pN applied force. An AFM probe with a colloidal tip, carefully positioned away from the cell boundary edges and away from the nucleus region **(A)**, was used as a nanoindentor to monitor changes in cell elasticity following decidualization. Using Sneddon mechanics, elasticity was calculated from the observed changes in the contact regime of the force curve (arrows in panel **B**), where two example approach curves are depicted here, on a control ESC (gray) and a decidualized cell (black). The 0 point in the x-axis indicates when the cantilever tip makes contact with the cell surface **(B)**. Total cell elasticity values are depicted in boxplots for control and decidualized cells at 72 h. **(C)** Highly significant alterations in median values ($P < 0.0001$) were detected between control (2.4 ± 0.1 kPa) and decidualized cells (1.1 ± 0.1 kPa). Indentation data are reported in **D**, where applying the same force results in decidualized cells deforming more than control cells (152 ± 7 nm and 89 ± 4 nm, respectively) ($P < 0.0001$). **(E)** Cantilever pull-off adhesion force, where both groups display non-specific adhesive properties ($P > 0.05$). Statistical significance was determined using the Mann–Whitney test, with the following used symbols: ns = $P > 0.05$ (threshold P value = 0.05); * = $P \leq 0.05$; ** = $P \leq 0.01$; *** = $P \leq 0.001$; **** = $P \leq 0.0001$.

instead a significantly lower stiffness (1.1 ± 0.1 kPa) compared to the control cells (2.4 ± 0.1 kPa, $P < 0.0001$). This mechanical transformation was mirrored in the identation data, where decidualized cells exhibited a significant higher deformation (152 ± 7 nm) compared to control cells (89 ± 4 nm). Consistent with sharp nanoscale indentors, no alteration in colloidal probe adhesion force was observed (Figure 6, *E*).

Here, two types of probes were used in order to characterize stiffness changes as cells undergo decidualization. Overall, a decrease in cell stiffness has been observed, which is more evident when colloidal probes were used, and was especially evident in the initial contact section of the approach curves (see Supplementary Figure 2). While the general trends observed between cell states with the two AFM probes were similar, the absolute values of both Young's modulus and indentation were different between sharp and colloidal probes (Figures 5 and 6): though the use of two different models (Sneddon and Hertz) accounts for some of this discrepancy, the significant decrease in Young's modulus when the colloidal probes were used is consistent with cellular biophysical trends in the literature. The reason underpinning it is still controversial and different hypotheses have been proposed,[18,21–24] among them strain stiffening.[25] This is determined by the higher pressure, sometimes more than one order of magnitude, exterted by the

sharp tip at the same applied force due to the lower contact area, which determines a counter reaction in the cell, with structure remodeling and localized surface stiffening.[25]

Discussion

Here we demonstrate distinct morphodynamic properties that characterize primary human ESCs during *in vitro* decidualization. Quantitative image analysis demonstrated changes in roundness and circularity, which were accompanied by alterations in the expression patterns of E-cadherin, N-cadherin and vimentin, hallmarks of the MET process. Driven by increased expression of dPRL, IGFBP-1 and EGFR, decidualization resulted in decreased cell stiffness, increased cellular indentation and a reduction in cell surface roughness. Such biophysical properties may potentially be important in the establishment of the unique environment necessary for the establishment and maintenance of pregnancy.

The increased circularity, height and elastic properties showed by decidualized ESCs in comparison to the control are likely due to the cytoskeletal changes promoted by MET (Figure 4).[26] These cytoskeletal readjustments, together with the vinculin redistribution and the F-actin destabilization, induce a change in cell morphology towards a more rounded form.[27] Unstimulated ESCs have the typical appearance of fibroblasts when imaged with AFM, Figure 4, *A-B*, with stress fibers visible below the cell membrane along the long axis of the cell.[28,29] A prominent MET cellular alteration, the switch between vimentin-rich and cytokeratin-rich networks, is represented by cytoskeletal reorganization.[11] The stress fibers are less visible following decidualization, where the cell surface consists of a dense mat of thinner fibers. Downregulation of the stress fibers, myosin light chain kinase (MLCK), α-smooth muscle actin, and the microtubule β-tubulin, decreases the cell surface roughness of ESCs after decidualization.[30] Thicker filaments are present near intercellular junctions, in agreement with F-actin organization for epithelial cells.[31]

Interestingly, cell surface roughness is thought to be an indicator of cell–cell adhesion. Decidualization resulted in decreased membrane roughness, which may result in increased cell–cell interaction consistent with biophysical properties previously reported.[32] Changes in F-actin and vinculin expression decrease focal adhesion capacity, defined as the adhesive contact between the cell and its substrate.[33] As a result, and despite the increased expression of E-cadherin, a protein involved in cell–cell adhesion, no significant alteration in ESC cellular adhesion was observed after decidualization. Consistently, Ihnatovych and colleagues showed no significant alteration in ESC adhesion following the induction of decidualization.[30]

Change in ESC stiffness upon *in vitro* decidualization was more evident with colloidal probe nanoindentation. Due to the interrogation of a larger surface area compared to the nanoscopic stiffness profiling when a sharp probe is used, colloidal probes are thought to produce a more accurate estimation of the overall cell stiffness.[21] Moreover, a better fitting of the Hertzian model to the experimental data usually occur, since this model uses a spherical indenter as well. It is also of significance to consider the close-to-spherical blastocyst contour, and how a spherical probe could be more appropriate to investigate in a more realistic way how decidualized cells respond to and interact with the implanting blastocyst.

The reduced stiffness phenotype of ESCs is most probably attributed to the downregulated expression of vimentin, previously shown to be associated with altered cell stiffness.[34] Actin fibers are also thought to be directly involved in cell stiffness, as decreased membrane stiffness is observed with actin depolymerisers.[35,36] The increased elastic phenotype correlates with cytoskeletal remodeling and increased decidualized cell height, a result of increased cell–cell interaction *via* enhancement of cell–cell adhesion and decreased cell flattening on the hard substrate surface.[37]

In addition, vimentin is thought to provide structural stability to the cell, its downregulation resulting in a phenotype less resistant to external stress, thereby encouraging blastocyst invasion.[38] Myosin light chain kinase downregulation has also been shown to result in a decrease in MLC_{20} phosphorylation, hampering actin–myosin interactions while enhancing epithelial permeability and favoring blastocyst invasion.[39] Moreover, it was found that decreased phosphorylation of MLC_{20} reduces cell stiffness contributing to decidualized ESC plasticity.[40]

Single cell mechanical changes in decidualized cells are in line with the supporting decidual layer hypothesis during embryo implantation. While known to support embryo attachment by interacting with trophoblast E-cadherin,[40,41] we believe that E-cadherin indicates gross tissue level alterations that contribute to a second stage of endometrial dynamics to constitute the essential barrier function. Decidualized endometrial tissue mechanics may be established *via* E-cadherin mediated force-sensitive complexes at intercellular junctions, which through interactions with α-catenin link to the actin cytoskeleton, resulting in altered cellular stiffness properties.[42–44] Alternatively, mechanotransduction could occur independently of α-catenin, through integrins, and require the activity of EGFR. Decidualization follows a wave of cell proliferation mediated by EGFR signaling. EGFR expression, as shown here, has also been demonstrated to be a critical factor involved in the amplification and maintenance of decidualization by inducing several signaling pathways implicated in altered biophysical signatures, including the c-Src kinase cascades, AKT/mTOR, STAT, MAPK and Wnt signaling.[45]

ESCs undergo a MET in response to the decidualization stimuli of cAMP and progesterone, a process contributed to by alterations in the expression of cytoskeletal and polarity complex proteins. Keratin and vimentin filaments regulate organelle and membrane-associated protein trafficking differentially targeting proteins such as E-cadherin to the cell membrane. For example, keratin, but not vimentin, directs E-cadherin to the membrane. Accompanied by the downregulation of mesenchymal N-cadherin this ‘cadherin switch’ alters cell adhesion by increasing the affinity of transitioning cells for epithelial cells through homotypic E-cadherin interactions. These interactions are stronger than homotypic N-cadherin interactions and facilitate epithelial barrier function,[46,47] enabling better control of the positioning and stabilization of the blastocyst.

Summary

Decidualization is a cellular process that is essential for embryo implantation and the subsequent establishment of pregnancy.[1] Decidualization appears to involve a spectrum of mechano-physical and biochemical changes and transitions that are dependent on the signaling context and local hormonal environment to establish a receptive uterine environment. This study reveals details of the cellular, molecular and mechanical changes that occur during *in vitro* ESC decidualization in the presence of cAMP. Identification of the correct nidation site is an essential, dynamic process in embryo apposition, while these data suggest that a bloated, softer underlying stroma, as a result of decidulaization, may well be an essential, closely timed state of differentiation required for correct invasion and subsequent establishment of pregnancy.

Impairment in the timing and state of differentiation of decidual cells has been observed in pathologies with altered etiology, including endometriosis, recurrent pregnancy loss, polycystic ovary syndrome (PCOS) and antiphospholipid syndrome (APLS), all of which are associated with diminished human reproductive potential. The approach adopted here will now be important in better determining how impaired decidualization may impact these diseases, particularly infertility, recurrent pregnancy loss and, subsequently, its effect on the efficiency of *in vitro* fertilization procedures.

Appendix A. Supplementary data

Supplementary data to this article can be found online at https://doi.org/10.1016/j.nano.2018.07.004.

References

1. Gellersen B, Brosens JJ. Cyclic decidualization of the human endometrium in reproductive health and failure. *Endocr Revg* 2014;**35**(6):851-905.
2. Christian M, Mak I, White JO, Brosens JJ. Mechanisms of decidualization. *Reprod Biomed Online* 2002;**4**(Suppl 3):24-30.
3. Dunn CL, Kelly RW, Critchley HOD. Decidualization of the human endometrial stromal cell: an enigmatic transformation. *Reprod Biomed Online* 2003;**7**(2):151-61.
4. Sharma S, Godbole G, Modi D. Decidual control of trophoblast invasion. *Am J Reprod Immunol* 2016;**75**(3):341-50.
5. Oreshkova T, Dimitrov R, Mourdjeva M. A cross-talk of decidual stromal cells, trophoblast, and immune cells: a prerequisite for the success of pregnancy. *Am J Reprod Immunol* 2012;**68**(5):366-73.
6. Pellicer A, Dominguez F, Remohi J, Simon C. Molecular basis of implantation. *Reprod Biomed Online* 2002;**5**(Suppl 1):44-51.
7. Cha J, Sun X, Dey SK. Mechanisms of implantation: strategies for successful pregnancy. *Nat Med* 2012;**18**(12):1754-67.
8. Gellersen B, Brosens IA, Brosens JJ. Decidualisation of the human endometrium: mechanisms, functions, and clinical perspectives. *Semin Reprod Med* 2007;**25**(6):445-53.
9. Gellersen B, Brosens J. Cyclic AMP and progesterone receptor cross-talk in human endometrium: a decidualizing affair. *J Endocrinol* 2003;**178**(3):357-72.
10. Large MJ, DeMayo FJ. The regulation of embryo implantation and endometrial decidualization by progesterone receptor signaling. *Mol Cell Endocrinol* 2012;**358**(2):155-65.
11. Zhang XH, Liang X, Liang XH, Wang TS, Qi QR, Deng WB, et al. The mesenchymal-epithelial transition during in vitro decidualization. *Reprod Sci* 2013;**20**(4):354-60.
12. Patterson AL, Zhang L, Arango NA, Teixeira J, Pru JK. Mesenchymal-to-epithelial transition contributes to endometrial regeneration following natural and artificial decidualization. *Stem Cells Dev* 2013;**22**(6):964-74.
13. Handorf AM, Zhou Y, Halanski MA, Li WJ. Tissue stiffness dictates development, homeostasis, and disease progression. *Organogenesis* 2015;**11**(1):1-15.
14. Noyes RW, Hertig AT, Rock J. Dating the endometrial biopsy. *Am J Obstet Gynecol* 1975;**122**(2):262-3.
15. Gonzalez D, Thackeray H, Lewis PD, Mantani A, Brook N, Ahuja K, et al. Loss of WT1 expression in the endometrium of infertile PCOS patients: a hyperandrogenic effect? *J Clin Endocrinol Metab* 2012;**97**(3):957-66.
16. Abràmofff MD, Magalhães PJ, Ram SJ. Image processing with ImageJ part II. *Biophotonics Int* 2005;**11**(7):36-43.
18. Harris AR, Charras GT. Experimental validation of atomic force microscopy-based cell elasticity measurements. *Nanotechnology* 2011;**22**(34).
21. Carl P, Schillers H. Elasticity measurement of living cells with an atomic force microscope: data acquisition and processing. *Pflugers Arch* 2008;**457**(2):551-9.
22. Dimitriadis EK, Horkay F, Maresca J, Kachar B, Chadwick RS. Determination of elastic moduli of thin layers of soft material using the atomic force microscope. *Biophys J* 2002;**82**(5):2798-810.
23. Costa KD, Yin FCP. Analysis of indentation: implications for measuring mechanical properties with atomic force microscopy. *J Biomech Eng* 1999;**121**(5):462-71.
24. Akhremitchev B, Walker G. Finite sample thickness effects on elasticity determination using atomic force microscopy. *Langmuir* 1999;**15**(17):5630-4.
25. Leporatti S, Gerth A, Köhler G, Kohlstrunk B, Hauschildt S, Donath E. Elasticity and adhesion of resting and lipopolysaccharide-stimulated macrophages. *FEBS Lett* 2006;**580**(2):450-4.
26. Garrido-Gomez T, Dominguez F, Quiñonero A, Diaz-Gimeno P, Kapidzic M, Gormley M, et al. Defective decidualization during and after severe preeclampsia reveals a possible maternal contribution to the etiology. *S A* 2017;**114**(40):E8468-77.
27. Zhu H, Hou C-C, Luo L-F, Hu Y-J, Yang W-X. Endometrial stromal cells and decidualized stromal cells: origins, transformation and functions. *Gene* 2014;**551**(1):1-14.
28. Braet F, de Zanger R, Seynaeve C, Baekeland M, Wisse E. A comparative atomic force microscopy study on living skin fibroblasts and liver endothelial cells. *J Electron Microsc (Tokyo)* 2001;**50**(4):283-90.
29. Rotsch C, Radmacher M. Drug-induced changes of cytoskeletal structure and mechanics in fibroblasts: an atomic force microscopy study. *Biophys J* 2000;**78**(1):520-35.
30. Ihnatovych I, Hu W, Martin JL, Fazleabas AT, de Lanerolle P, Strakova Z. Increased phosphorylation of myosin light chain prevents in vitro decidualization. *Endocrinology* 2007;**148**(7):3176-84.
31. Millán J, Cain RJ, Reglero-Real N, Bigarella C, Marcos-Ramiro N, Fernández-Martín L, et al. Adherens junctions connect stress fibres between adjacent endothelial cells. *BMC Biol* 2010;**8**:11.
32. Le Guehennec L, Lopez-Heredia M-A, Enkel B, Weiss P, Amouriq Y, Layrolle P. Osteoblastic cell behaviour on different titanium implant surfaces. *Acta Biomater* 2008;**4**(3):535-43.
33. Ahmad Khalili A, Ahmad MR. A review of cell adhesion studies for biomedical and biological applications. *Int J Mol Sci* 2015;**16**(8):18149-84.
34. Wang N, Stamenović D. Contribution of intermediate filaments to cell stiffness, stiffening, and growth. *Am J Physiol Cell Physiol* 2000;**279**(1):C188-94.
35. Charras GT, Horton MA. Single cell mechanotransduction and its modulation analyzed by atomic force microscope indentation. *Biophys J* 2002;**82**(6):2970-81.

36. Ketene AN, Roberts PC, Shea AA, Schmelz EM, Agah M. Actin filaments play a primary role for structural integrity and viscoelastic response in cells. *Integr Biol (Camb)* 2012;**4**(5):540-9.
37. Kondo T, Hayashi S. Mechanisms of cell height changes that mediate epithelial invagination. *Dev Growth Differ* 2015;**57**(4):313-23.
38. Ivaska J, Pallari H-M, Nevo J, Eriksson JE. Novel functions of vimentin in cell adhesion, migration, and signaling. *Exp Cell Res* 2007;**313**(10):2050-62.
39. Gandhi S, Lorimer DD, de Lanerolle P. Expression of a mutant myosin light chain that cannot be phosphorylated increases paracellular permeability. *Am J Physiol* 1997;**272**(2 Pt 2):F214-21.
40. An SS, Laudadio RE, Lai J, Rogers RA, Fredberg JJ. Stiffness changes in cultured airway smooth muscle cells. *Am J Physiol Cell Physiol* 2002;**283**(3):C792-801.
41. Horne AW, White JO, Lalani E-N. Adhesion molecules and the normal endometrium. *BJOG* 2002;**109**(6):610-7.
42. Barry AK, Tabdili H, Muhamed I, Wu J, Shashikanth N, Gomez GA, et al. alpha-catenin cytomechanics—role in cadherin-dependent adhesion and mechanotransduction. *J Cell Sci* 2014;**127**(Pt 8):1779-91.
43. le Duc Q, Shi Q, Blonk I, Sonnenberg A, Wang N, Leckband D, et al. Vinculin potentiates E-cadherin mechanosensing and is recruited to actin-anchored sites within adherens junctions in a myosin II-dependent manner. *J Cell Biol* 2010;**189**(7):1107-15.
44. Thomas WA, Boscher C, Chu YS, Cuvelier D, Martinez-Rico C, Seddiki R, et al. alpha-Catenin and vinculin cooperate to promote high E-cadherin-based adhesion strength. *J Biol Chem* 2013;**288**(7):4957-69.
45. Large MJ, Wetendorf M, Lanz RB, Hartig SM, Creighton CJ, Mancini MA, et al. The epidermal growth factor receptor critically regulates endometrial function during early pregnancy. *PLoS Genet* 2014;**10**(6)e1004451.
46. Wheelock MJ, Shintani Y, Maeda M, Fukumoto Y, Johnson KR. Cadherin switching. *J Cell Sci* 2008;**121**(Pt 6):727-35.
47. Lamouille S, Xu J, Derynck R. Molecular mechanisms of epithelial-mesenchymal transition. *Nat Rev Mol Cell Biol* 2014;**15**(3):178-96.